Phase diagrams and critical behavior of Ising square lattices with nearest-, next-nearest-, and third-nearest-neighbor couplings

D. P. Landau* and K. Binder†
Department of Physics and Astronomy, University of Georgia, Athens, Georgia 30602
and Institut für Festkörperforschung, der Kernforschungsanlage Jülich, 5170 Jülich Postfach 1913, Federal Republic of Germany
(Received 21 November 1984)

Monte Carlo simulations are used to study the location and nature of phase boundaries for Ising square lattices with antiferromagnetic coupling J_{NN} between nearest neighbors and additional interactions J_{NNN} between next-nearest neighbors and J_{3NN} between third-nearest neighbors. Results in zero magnetic field are obtained for a wide range of $R=J_{NNN}/J_{NN}$ and $R'=J_{3NN}/J_{NN}$. In addition to the $c(2\times2)$ and (2×1) phases, which also occur for $R'=0$, we find new (4×4) and (4×2) ordered states, for $R'\neq0$, which are separated from the disordered state by lines of first-order transitions. The nonuniversal critical behavior of the (2×1) phase is studied using the block-distribution method and finite-size scaling. The possible existence of incommensurate phases is also explored.

I. INTRODUCTION

The Ising square lattice has long been the object of scrutiny. Although it can be solved analytically[1] when nearest-neighbor (NN) coupling is present, the model has defied solution when more-distant-neighbor interactions are added. For many years the model was of purely theoretical interest, but more recently it has been recognized that both layered quasi-two-dimensional anisotropic antiferromagnets[2–4] and adsorbed monolayers on cubic (100) surfaces[5–7] may be describable in terms of this model. Because of this a wide variety of approximate methods have been applied to the model: mean-field theory,[8,9] series expansions,[10–13] real-space renormalization-group methods,[14–19] interface methods,[20–22] free-fermion calculations,[23] and Monte Carlo and Monte Carlo renormalization-group (MCRG) computer simulations.[24–27]

We now know that if next-nearest-neighbor (NNN) coupling is added the ground state may be either $c(2\times2)$, with the usual Ising exponents, or (2×1) with nonuniversal critical behavior, i.e., exponents which depend upon $R=J_{NNN}/J_{NN}$. (In Fig. 1 we show a number of possible ground-state configurations and label them with both the usual magnetic designation as well as that used for describing adsorbed monolayers.) The effects of adding third-nearest-neighbor (3NN) coupling, however, is not yet generally understood. Selke and Fisher[28] have given preliminary phase boundaries for the special case of NN and 3NN coupling. This model, which is an isotropic version of the axial NNN Ising (ANNNI) model, shows an incommensurate phase in addition to ordered, commensurate phases.

In this paper we shall describe the results of extensive Monte Carlo calculations on this model. From these data we shall locate phase boundaries, determine their character, and compare the results with the predictions based on ground-state symmetry arguments.[29] In Sec. II we present ground-state and mean-field results for this model. In Sec. III we describe the methods used to obtain and analyze data. Section IV gives our conclusions.

II. THEORETICAL BACKGROUND

We consider Ising square lattices with the Hamiltonian

$$\mathcal{H}=J_{NN}\sum_{NN}\sigma_i\sigma_j+J_{NNN}\sum_{NNN}\sigma_i\sigma_k+J_{3NN}\sum_{3NN}\sigma_i\sigma_l\ , \qquad (1)$$

where $\sigma_i=\pm1$ and the sums are over NN, NNN, and 3NN pairs, respectively. The ground-state energies of the ordered states shown in Fig. 1, as well as many other possible ordered states, were calculated. We find that states

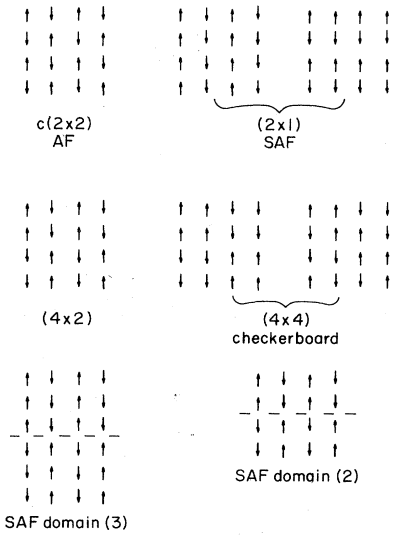

FIG. 1. Possible ground-state spin configurations on the square lattice. Both lattice-gas and magnetic notation are shown where appropriate.

with the lowest energies for some region of R and R' have energies

$$\frac{U_0^{c(2\times2)}}{|J_{NN}|}=-2+2R+2R', \tag{2a}$$

$$\frac{U_0^{(2\times1)}}{|J_{NN}|}=-2R+2R', \tag{2b}$$

$$\frac{U_0^{(4\times4)}}{|J_{NN}|}=-2R', \tag{2c}$$

$$\frac{U_0^{(4\times2)}}{|J_{NN}|}=-1. \tag{2d}$$

By comparing these energies we find a ground-state phase diagram as shown in Fig. 2. (Our results agree with those of Kaburagi[30] who approached this problem somewhat differently.) Using mean-field theory, we also find indications of interesting behavior for $T>0$. In mean-field theory the momentum-space susceptibility can be written

$$\chi(\bar{q})=\frac{\mu^2}{k_BT-J(\bar{q})}. \tag{3}$$

For the model which we are considering,

$$J(\bar{q})=2\{J_{NN}(\cos q_x+\cos q_y)+J_{NNN}[\cos(q_x+q_y)+\cos(q_x-q_y)]+J_{3NN}[\cos(2q_x)+\cos(2q_y)]\}. \tag{4}$$

The (2×1) phase corresponds to $q_x=\pi$, $q_y=0$ or $q_x=0$, $q_y=\pi$. By writing out $J(q)$ explicitly for small deviations from the q for the (2×1) phase, we find that an incommensurate phase becomes stable for $2J_{NNN}-J_{NN}-4J_{3NN}>0$; hence a Lifshitz point appears for $R'_{Lif}=\frac{1}{2}R-\frac{1}{4}$. This behavior is quite similar to that of the ANNNI model (in fact our model may be considered to be a generalization of the isotropic version of the ANNNI model). The qualitative phase diagram that we might then expect is shown in Fig. 3. In the mean-field case the incommensurate phase also makes transitions to various commensurate phases [including (4×4) at low temperatures] when the temperature is sufficiently lower than the paramagnetic-incommensurate transition.[31] Since the phase diagram is expected to be very complicated ("devil's staircase" of phases), no attempt to include these phases has been made.

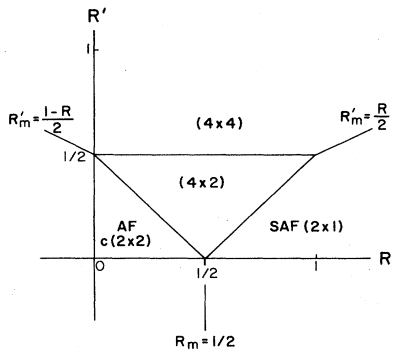

FIG. 2. Phase diagram at $T=0$.

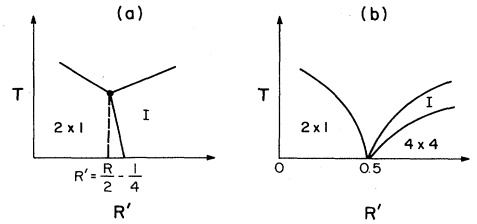

FIG. 3. Possible phase diagrams showing an incommensurate phase: (a) schematic (simplified) mean-field diagram; (b) phase diagram from Monte Carlo calculations of Ref. 28.

III. SIMULATION METHODS

A. Monte Carlo method

Data have been obtained using a standard importance-sampling Monte Carlo method which employs single spin-flip kinetics.[32] We have studied $L\times L$ lattices with periodic boundary conditions for lattices as large as $L=48$. Phase boundaries were generally located using data points obtained from 400 MCS (Monte Carlo steps per spin). Data obtained for analysis of critical point behavior using the block distribution (cumulant) method[33] (to be described below) employed much longer runs. Typically for $L=4$ we kept 10^5 MCS for calculating the cumulants and for $L=32$ about 1.5–2.0×10^4 MCS were kept. Each point was then repeated at least once and the results averaged.

B. Free-energy analysis near first-order transitions

The bulk properties of a system exhibiting a first-order transition will often exhibit hysteresis. The actual loca-

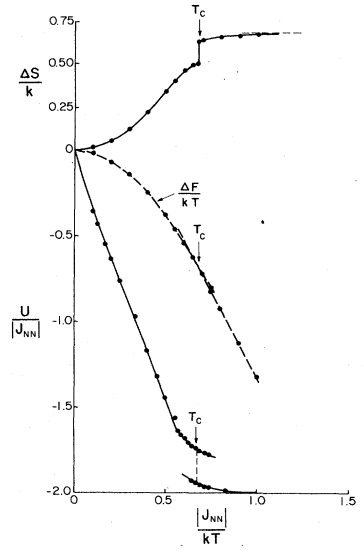

FIG. 4. Determination of the location of the first-order phase transition for $R=\frac{1}{2}$, $R'=1$ from comparison of free energies. The upper part of the diagram shows the entropy determined via this procedure.

tion of the transition may then be determined directly from the Monte Carlo data. If, however, the hysteresis is extremely pronounced, this description may be difficult (or even impossible) to use. Instead, one may determine the location of the transition through an analysis of the free energy F and entropy S as described by Binder.[34] The internal energy U is integrated starting at infinite temperature, yielding

$$\frac{F}{k_B T} = -S(T=\infty) + \int_0^{1/k_B T} U d(1/k_B T) \tag{5}$$

and

$$\frac{S}{k_B} = \frac{S(T=\infty)}{k_B} + \frac{U}{k_B T} - \int_0^{1/k_B T} U d(1/k_B T) . \tag{6}$$

At a first-order transition there will be a jump ΔU in the internal energy which gives rise to a jump in the entropy $\Delta S = \Delta U / k_B T$. The transition temperature must then be chosen consistent with the restriction that the total entropy determined from the integration is exactly equal to the exact value determined from the spin degeneracy (for example, in the present case $S(T=\infty)/k_B = \ln 2$). Figure 4 shows a practical example.

C. Block distribution (cumulant) analysis

If the magnetic field is zero, the spin distribution function $P_L(s)$ for an $L \times L$ lattice is symmetric, i.e.,

$$P_L(s) = P_L(-s) . \tag{7}$$

The expectation value of the kth spin moment is then given by[33]

$$\langle s^k \rangle_L = \int ds\, s^k P_L(s) . \tag{8}$$

An analogous expression can be written in terms of a more general order parameter m which is appropriate to nonferromagnetic order

$$\langle m^k \rangle_L = \int dm\, m^k P_L(m) . \tag{9}$$

Following Ref. 33 we can define cumulants as well:

$$U_L = 1 - \frac{\langle m^4 \rangle_L}{3 \langle m^2 \rangle_L^2} . \tag{10}$$

The critical behavior can then be determined from a comparison of the moments and cumulants for lattices of size L and $L' = bL$. At T_c

$$U_L = U_{L'} = U^* , \tag{11}$$

$$\nu^{-1} = \frac{\ln(\partial U_{bL} / \partial U_L)_{U^*}}{\ln b} , \tag{12}$$

and

$$\frac{2\beta}{\nu} = \ln(\langle m^2 \rangle_{bL} / \langle m^2 \rangle_L) / \ln b . \tag{13}$$

Since there are in general residual effects due to corrections to finite-size scaling, it is necessary to extrapolate the results as a function of $(\ln b)^{-1}$ to $(\ln b)^{-1} = 0$. For practical examples, see Figs. 11 and 12 below.

D. Finite-size scaling

The behavior of finite systems near the infinite lattice critical temperature can be described by finite-size scaling theory.[35] For example, for sufficiently large values of L the specific heat should diverge as $L^{\alpha/\nu}$, where α and ν are the infinite lattice exponents. If we interpret the location of the specific-heat peak as the finite lattice critical temperature $T_c(L)$, then

$$\frac{k_B [T_c(L) - T_c(\infty)]}{J_{NN}} = a L^{1/\nu} . \tag{14}$$

In addition, at $T_c(\infty)$ the order parameter should go to 0 as $L^{-\beta/\nu}$. The analysis of the size dependence of these properties has been quite successful in the determination of infinite lattice critical exponents.[36]

IV. RESULTS

A. Phase diagrams

We have chosen a number of different values of R for which different characteristic behavior is found as a function of R' and have determined the critical temperatures as a function of R'. In Fig. 5 we show the phase diagrams for $R = 1.5$ and $R = 1.0$ for which only the staggered antiferromagnetic (SAF) (2×1) and (4×4) ordered structures appear at low temperatures. The phase transition involving the SAF state was clearly second order. The transition from the (4×4) state to the disordered state was strongly first order at low temperatures, and the transition temperature could be determined only by comparison of free energies. At higher temperatures the hysteresis became much less pronounced and T_c could be determined directly. No incommensurate phase in between the (4×4) phase and disordered phase was found.

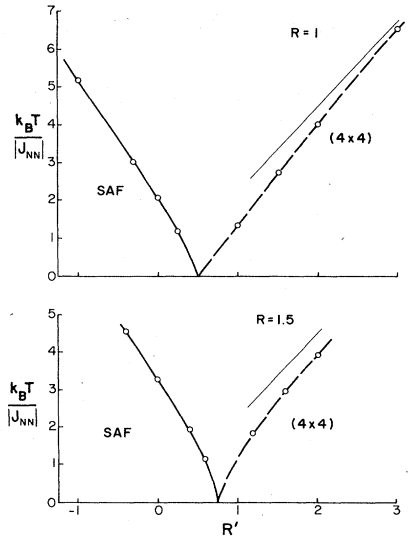

FIG. 5. Phase diagrams for $R = 1$ and $R = 1.5$ showing the phase boundaries to the SAF and (4×4) phases as a function of R'. Results are for $L = 48$. The thin solid lines show the asymptotic behavior for $R' \to \infty$.

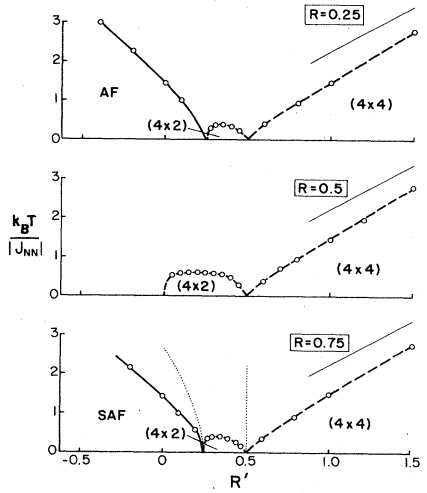

FIG. 6. Phase diagrams for $R=0.25$, 0.5, and 0.75 showing phase boundaries to the AF, SAF, (4×2), and (4×4) phases as a function of R'. Results are for $L=48$. The thin solid lines show the asymptotic behavior for $R'\to\infty$. The dotted curves shown for $R=0.75$ separate the regions of short-range order of different types.

This behavior is in contrast to that observed previously for the isotropic ANNNI model.[28] Due to its large unit cell, the (4×4) state has a large number of order-parameter components. Thus it is clear that this phase cannot belong to any of the orderings for which symmetry arguments[29] would predict a second-order transition to the disordered state.

In Fig. 6 we show phase diagrams for $R=0.25$, 0.5, and 0.75. All three phase diagrams show a line of first-order transitions from the (4×4) state to the disordered states; these phase boundaries are qualitatively similar to those in Fig. 5. For all three values of R we also observe a (4×2) ordered state which is also separated from the disordered phase by a line of first-order transitions. The transition was also strongly first order at low temperatures and T_c could be determined only by comparison of free energies. The major qualitative differences in these phase diagrams is the appearance of an ordered antiferromagnetic $c(2\times2)$ phase for $R=0.25$ and a SAF (2×1) phase for $R=0.75$. No corresponding phase is present for $R=0.5$. Recall that at this value both phases are degenerate in the ground state. Thus it is quite plausible that at finite temperature fluctuations can destabilize any order. In Fig. 7 we show phase diagrams for these values of $R\leq0$. The phase diagrams are qualitatively alike with second-order transitions to an antiferromagnetic (AF) $c(2\times2)$ state and first-order transitions to the (4×4) state. At low temperatures the (4×4) phase boundaries seem to show small "bulges"; these protrusions and their implication for the nature of the phase boundary will be discussed shortly.

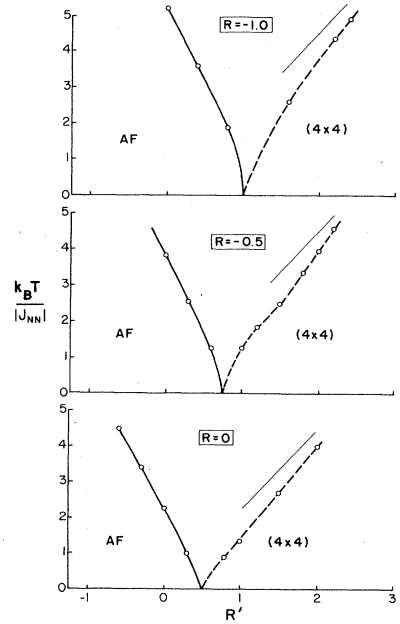

FIG. 7. Phase diagrams for $R=-1.0$, -0.5, and 0 showing the phase boundaries to the AF and (4×4) phases as a function of R'. Results are for $L=48$. The thin solid lines show the asymptotic behavior for $R'\to\infty$.

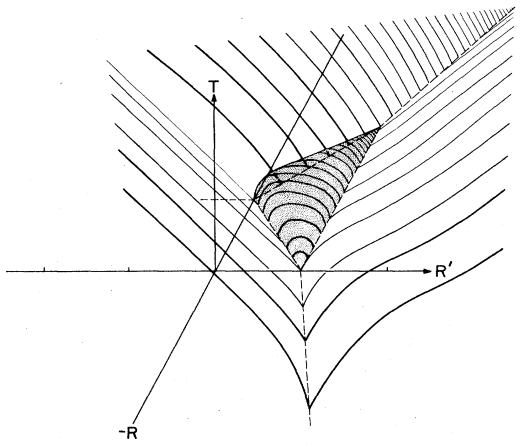

FIG. 8. R-R'-T phase diagram.

Using the results just presented, we have constructed a three-dimensional phase diagram in R-R'-T space. This is shown in Fig. 8. The shaded "bubble" in the center is the surface bounding the (4×2) phase; the dashed lines show the $T=0$ phase boundaries which are in the R-R' plane.

B. Critical behavior

1. The checkerboard phase

A careful study of the nature of the transition from the checkerboard (4×4) to the disordered phase is interesting for several reasons. Previous work by Selke and Fisher[28] on the isotropic ANNNI model (our model with $R=0$, $R'>0$) suggested that as the temperature increases the system first enters an incommensurate phase after which it undergoes a second transition to the disordered state. However, Selke and Fisher studied only one lattice size for this model; experience with the ANNNI model shows, however, that a finite-size analysis is crucial for any de-

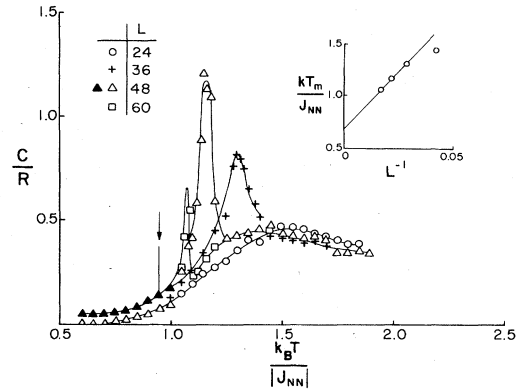

FIG. 9. Specific heat for $R=0$, $R'=0.8$. The arrow shows the location of the transition to the commensurate, ordered state, as determined from the free energy. The solid triangles show the specific heat obtained as the temperature is reduced from above. The inset shows an extrapolation of the temperature T_m at which the upper specific-heat peak occurs.

finite statement about the existence of an incommensurate phase. Since the checkerboard state is stable over a wide range of the interaction space which we have studied, and the phase boundaries showed unusual bulges as $T_c \to 0$, it seemed particularly important to determine whether this incommensurate phase really existed. With this goal in mind we have carried out a more detailed analysis of the phase transitions involving the (4×4) state and in particular have investigated the effects of finite size. In Fig. 9 we show the variation of the specific heat with temperature over a wide range of lattice sizes. For a (12×12) lattice we see a rounded specific-heat peak located about $k_BT/|J_{NN}| \sim 1.5$ with very large values occurring at a clearly first-order transition (with hysteresis) at a much lower temperature.

As the lattice size increases the rounded peak changes only slightly, but a second relatively sharp peak grows very quickly and shifts to lower temperature. The hysteresis at the low-temperature transition becomes so pronounced that the system never reaches the ground state as the temperature is lowered and remains trapped in a metastable state. The location of this first-order transition was determined by integration of the free energy and we estimate $k_BT_c/J_{NN}=0.95$. The location of the second transition T_c was determined from the specific-heat peaks and extrapolated to $L=\infty$. A fairly wide range of power laws could be used to carry out this extrapolation; in the inset to Fig. 9 we show an extrapolation versus L^{-1} which yields an infinite lattice value of $k_BT_c/J_{NN} \sim 0.7$.

There is no *a priori* knowledge of the asymptotic size dependence, but we certainly would not expect T_c to vary faster than L^{-2} (i.e., a first-order transition), which yields $k_BT_c/J_{NN} \sim 0.9$. In all cases it appears that the extrapolated upper critical temperature for the incommensurate phase lies below the first transition to the ordered (4×4). Calculations of the structure factor show slight evidence for short-range order of a modulated type above the ordered (4×4) regime but no modulated phase. We therefore conclude that the incommensurate phase does not exist and the system undergoes a single order-disorder transition which is of first order. Similar finite-size behavior was found for other values of R' and it would seem likely that all transitions for the (4×4) state in this model are the same.

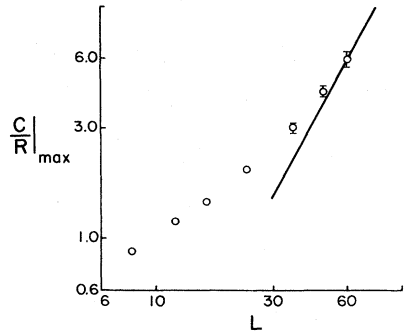

FIG. 10. Size dependence of the specific-heat peak for $R=0$, $R'=2.0$. The solid line has slope = 2.

For larger values of R' the hysteresis becomes less and less pronounced until it apparently disappears by the time $R'=2.0$. This behavior might be interpreted as suggesting that a tricritical point appears on the phase boundary for $R' \lesssim 2.0$. We investigated this possibility by carrying out a careful finite-size study of the transition behavior for $R'=2$. For small lattices the specific-heat peak increases relatively slowly with increasing L, as shown in Fig. 10; however, as the lattice becomes even larger, the size dependence becomes more pronounced and by the time $L \sim 60$ it would appear to be consistent with the L^2 variation expected at a first-order transition.[37] The same behavior can be seen in the variation of the critical temperature. Further study for larger R' seems futile since the system should be less first-order-like and we would need much larger lattices to see the asymptotic regime.

2. *The SAF phase*

The phase boundary separating the SAF (2×1) state from the disordered phase is now known to exhibit

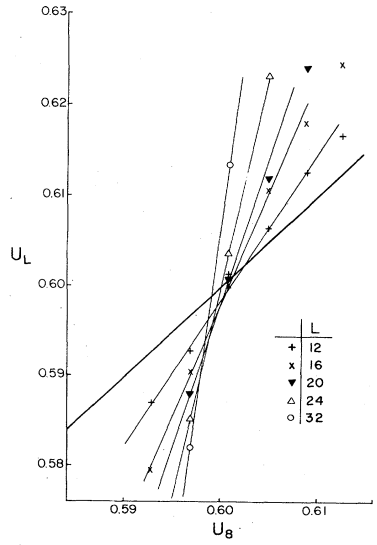

FIG. 11. Dependence of the cumulant U_L on lattice size for $R=0.65$, $R'=0$.

nonuniversal critical behavior. A number of studies have now been carried out for varying R with $R'=0$; we have therefore studied this phase boundary in detail using the block distribution method described in Sec. II. In order to assess the error estimates of this analysis we chose one value, $R=0.65$, to study with very long runs. For $L=4$ a total of 2×10^6 MCS were used with the runs decreasing in length until for $L=32$ a total of 3×10^5 MCS were kept for the averages. In Fig. 11 we show results for U_L versus U_8 for $12\leq L\leq 32$. The thin solid lines show linear fits to the data close to the critical temperature, i.e., close to the intersection with the line of slope 1. The variation of the critical temperature and critical exponents with the scale factor $b=L/L'$ which relates the two lattices being compared is shown in Fig. 12. The extrapolations for $L'=8$ and $L'=12$ agree quite well; the difference for $L'=4$ suggests that the lattice sizes studied are not yet in the asymptotic regime where the effects of correction terms to finite-size scaling justify a strictly linear extrapolation.

Our extrapolated results for a wide range of R are shown in Fig. 13 along with results obtained using other methods. The agreement with the MCRG results is quite good, and both sets of estimates for ν lie outside the predictions obtained from series expansions. The finite strip RG estimates for ν appear to be quite good; however, the critical temperatures were not given in Ref. 16 and the estimates were hence obtained using our estimates for T_c. For all values of R the estimates for $2\beta/\nu$ fell within the range 0.23 ± 0.03 with no systematic variation with R.

The fixed-point cumulant U^* also varies substantially with R. The results for $R'=0$, see Fig. 14, show a rapid drop as $R\to0.5$. For large R the value of U^* rises slightly above the estimate for the nearest-neighbor square lattice. This means that either U^* does not approach the $R=\infty$ limit monotonically with increasing R or that finite-size corrections are still sufficiently strong that we have not really reached the regime of asymptotic behavior for the lattice sizes studied here.

Estimates can also be extracted from the size dependence of bulk properties as described in Sec. III D. Using the estimate of $T_c(\infty)$ extracted from Fig. 12, we constructed a plot of $\ln k_B[T_c(L)-T_c(\infty)]/J_{NN}$ versus $\ln L$ for $R=0.75$, $R'=0$. This plot, shown in Fig. 15, does indeed show the variation predicted in Eq. (14) and yields $\nu=0.65$. From the variation of the specific-heat maxima, also shown in Fig. 15, we find $\alpha/\nu=0.92$. Combined with the scaling law $d\nu=2-\alpha$, this estimate yields $\nu=0.68$. These values are in close agreement with the result obtained in Fig. 12 from the cumulant. The size dependence of the order parameter shown in Fig. 15 is consistent with a "universal" value of $2\beta/\nu=0.25$.

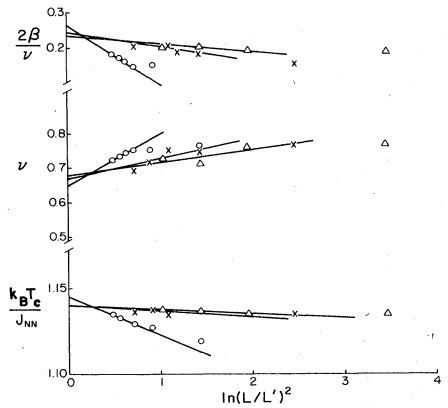

FIG. 12. Variation of critical parameters with $b=L/L'$ for $R=0.65$, $R'=0$. Data for ○, $L=4$; ×, $L=8$; △, $L=12$.

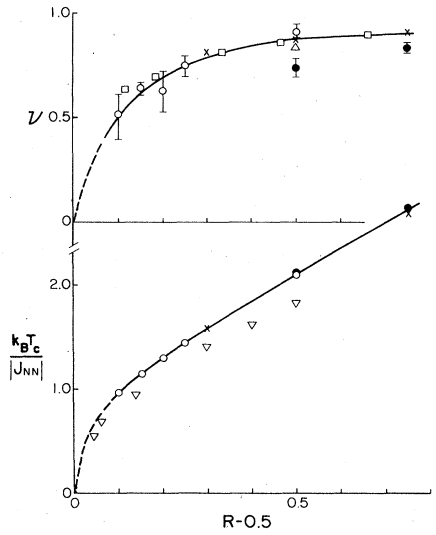

FIG. 13. Variation of the correlation length exponent and critical temperature T_c with R for $R'=0$. Results of the present block distribution Monte Carlo study, ○; Monte Carlo result from Ref. 26, △; MCRG results of Swendsen and Krinsky (Ref. 27, ×; series-expansion results of Ref. 13, ●; finite strip RG (Ref. 16), □; real space RG results of Ref. 15, ▲.

C. First-order behavior

Since the $(4\times2)\to P$ and $(4\times4)\to P$ transitions are first order, there are no characteristic exponents which can be used to describe the transitions. We can, however, examine the discontinuities in the bulk properties which occur at the transitions. These do indeed show a characteristic behavior, an example of which is shown in Fig. 16. For

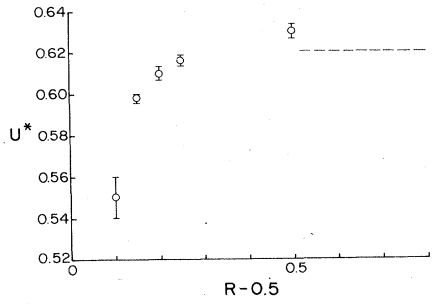

FIG. 14. Variation of the fixed point value of the cumulant U^* with R. The dashed line shows the result for $R=0$.

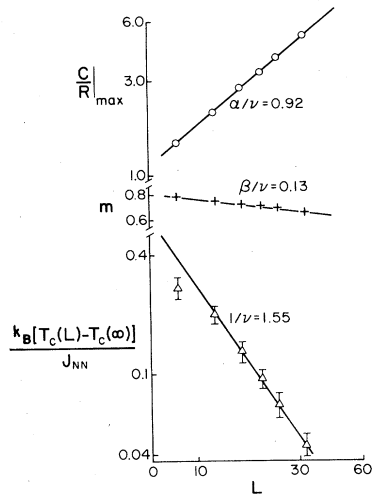

FIG. 15. Finite-size dependence of critical behavior for $R=0.65$, $R'=0$.

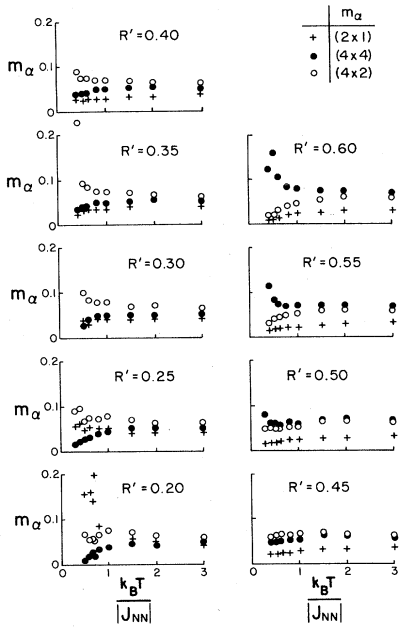

FIG. 17. Temperature dependence of order parameters for $L=36$ and $R=0.75$.

the $(4\times2)\rightarrow P$ transition the discontinuities in the internal energy, which corresponds to the latent heat in the specific heat, and the entropy show rounded maxima as a function of R. For the (4×4) transition, however, the internal energy discontinuity increases monotonically with R' over the range studied, but the entropy shows a broad maximum at about $R'\sim1$. Note that the magnitude of the discontinuity in the entropy is generally much greater for the transition to the (4×2) state than for the (4×4) state although the reverse is true for the internal energy. The order-parameter discontinuities at the transitions are all quite large (>0.95) for the values of R' studied for the (4×2) transition. For the (4×4) transition the discontinuity is quite large for R' near 0.5 but then begins to decrease for large R'. In the limit $R'\rightarrow\infty$ the lattice breaks up into four interpenetrating, noninteracting Ising square lattices (with twice the lattice constant of the original system) which undergo simultaneous second-order transitions to the disordered state. It is therefore necessary that $\Delta m\rightarrow0$ and $\Delta S\rightarrow0$ in this limit; since the ground-state energy, $U_0\rightarrow\infty$ as $R\rightarrow\infty$, it is also necessary that $\Delta U/U_0\rightarrow0$, and from Fig. 16 and Eq. (2c) we see that this is indeed the case. The behavior of the discontinuities

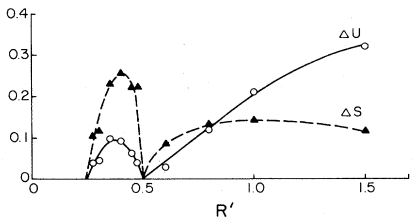

FIG. 16. Variation of the discontinuities in the internal energy $\Delta U/R$ and the entropy $\Delta S/R$ at the first-order phase transitions for $R=0.75$.

of other values of R' is qualitatively similar to that just presented.

D. Short-range order and disorder points

Above the phase boundaries the system is in a disordered state but one which can show considerable short-range order. For phase diagrams with multiple-ordered phases, such as those shown in Fig. 6, it is not obvious how the short-range order will vary with T and R'. To examine this behavior we have taken data for $R=0.75$ and have plotted the order parameters (for all three states which show order) as a function of temperature in Fig. 17. Since we are looking at finite ($L=36$) systems the order parameter, of type m_α, is a measure of the correlation between two sites a distance $L/2$ apart. For $R>0.5$ $m_{4\times4}$ is larger than $m_{4\times2}$ at all temperatures, for $R=0.5$ they are almost the same, and for $R'<0.45$ $m_{4\times2}$ is greater than $m_{4\times4}$ at all temperatures. For $R'<0.25$ we find that $m_{4\times2}$ is greatest at high temperature, but that as the temperature is lowered $m_{2\times1}$ becomes larger and remains so down to the phase transition. Since the (4×2) state shows a greater periodicity in the (11) direction than does the (2×1) state, this behavior may be analogous to the disorder point behavior described by Stephenson.[38] Stephenson showed rigorously that in the triangular Ising antiferromagnet there exists a temperature T_d in the disordered phase where the asymptotic exponential decay of the correlations changes from oscillatory in sign (characteristic of antiferromagnetic short-range order) to monotonically positive (characteristic of ferromagnetic short-range order). In our case we expect disorder lines separating asymptotic decays characteristic of the various types of AF order as well.

V. CONCLUSIONS

We have determined the location and nature of the zero-field phase transitions which occur over a wide range of R and R'. Depending on the values of these parameters, the system may order in various antiferromagnetic structures, namely $c(2\times2)$, (2×1), (4×2), and (4×4) phases in the notation of Fig. 1 or stay disordered at all temperatures (this happens only for special values of R,R'). We find that transitions from the disordered states to the (4×2) and (4×4) phases are first order. We also conclude that in an infinite system there is no incommensurate phase although in a finite system the data could be interpreted as showing an incommensurate phase. We have also studied the nonuniversal critical behavior for the transition from the SAF state to the paramagnetic state. We find no evidence for any order-order transition between any of the ordered phases. Since unit cells as large as (4×4) are needed to describe the ordered states, which are in many cases degenerate, we believe the behavior in a field is likely to be quite rich and we are currently in the process of studying it. This problem would possibly be experimentally relevant for adsorbed monolayers on (100) surfaces of cubic metals which might be modeled by the corresponding lattice gas.

ACKNOWLEDGMENTS

We thank W. Selke for useful comments. This work was supported in part by National Science Foundation (NSF) Grant No. DMR-8300754 by NATO Grant No. 064.82 and by the Program in Simulational Physics at the University of Georgia.

---

*Permanent address: Department of Physics and Astronomy, University of Georgia, Athens, GA 30602.

†Present address: Institut für Physik, Universitat Mainz, Postfach 3980, D-6500 Mainz, W. Germany.

[1]L. Onsager, Phys. Rev. **65**, 117 (1944); for a complete review, see B. M. McCoy and T. T. Wu, *The Two-Dimensional Ising Model* (Harvard University Press, Cambridge, Mass., 1973).

[2]L. J. de Jongh and A. R. Miedema, *Experiments on Simple Magnetic Model Systems* (Taylor and Francis, London, 1974).

[3]H. Ikeda and K. Hirakawa, Solid State Commun. **14**, 529 (1974).

[4]E. J. Samuelsen, J. Phys. Chem. Solids **35**, 785 (1974).

[5]K. Binder and D. P. Landau, Surf. Sci. **61**, 577 (1976).

[6]G. Doyen, G. Ertl, and M. Plancher, J. Chem. Phys. **62**, 2975 (1975); G. Ertl and M. Plancher, Surf. Sci. **48**, 364 (1974); G. Ertl and J. Küppers, *ibid.* **21**, 61 (1970).

[7]D. E. Andersson and S. Andersson, Surf. Sci. **23**, 311 (1970).

[8]J. S. Smart, *Effective Field Theories in Magnetism* (Saunders, London, 1966).

[9]S. Katsura and S. Fujimori, J. Phys. C **7**, 2506 (1974).

[10]D. C. Rapaport and C. Domb, J. Phys. C **4**, 2684 (1971).

[11]N. W. Dalton and D. W. Wood, J. Math. Phys. **10**, 1271 (1969).

[12]M. Plischke and J. Oitmaa, Phys. Rev. B **19**, 487 (1979).

[13]J. Oitmaa, J. Phys. A **14**, 1159 (1981).

[14]B. Nienhuis and M. Nauenberg, Phys. Rev. B **13**, 2021 (1976).

[15]M. Nauenberg and B. Nienhuis, Phys. Rev. Lett. **33**, 944 (1974).

[16]M. P. Nightingale, Phys. Lett. **59A**, 486 (1977).

[17]B. Schuh, Z. Phys. **31**, 55 (1978).

[18]K. R. Subbaswamy and G. D. Mahan, Phys. Rev. Lett. **37**, 642 (1976).

[19]W. Kinzel, Phys. Rev. B **19**, 4584 (1979).

[20]E. Müller-Hartmann and J. Zittartz, Z. Phys. B **27**, 261 (1977).

[21]T. W. Burkhardt, Z. Phys. B **29**, 129 (1978).

[22]B. W. Southern, Z. Phys. B **30**, 61 (1978).

[23]R. W. Gibberd, J. Math. Phys. **10**, 1026 (1969); C. Fan and F. Y. Wu, Phys. Rev. **179**, 560 (1969); A. Kawasaki and T. Osawa, J. Phys. Soc. Jpn. Suppl. **26**, 105 (1969).

[24]D. P. Landau, J. Appl. Phys. **42**, 1284 (1971).

[25]D. P. Landau, Phys. Rev. B **21**, 1285 (1980).

[26]K. Binder and D. P. Landau, Phys. Rev. B **21**, 1941 (1980).

[27]R. H. Swendsen and S. Krinsky, Phys. Rev. Lett. **43**, 177 (1979).

[28]W. Selke and M. W. Fisher, Z. Phys. B **40**, 71 (1980).

[29]E. Domany, M. Schick, J. S. Walker, and R. B. Griffiths, Phys. Rev. B **18**, 2209 (1978).

[30]M. Kaburagi, J. Phys. Soc. Jpn. **44**, 54 (1978); J. Kanamori and M. Kaburagi, *ibid.* **52**, 4184 (1983); U. Brandt, Z. Phys. B **53**, 283 (1983).

[31]See, e.g., W. Selke and P. M. Duxbury, Z. Phys. B **57**, 49 (1983), and references therein.

[32]For details on this method, see *Monte Carlo Methods in Statistical Physics,* Vol. 7 of *Topics in Current Physics,* edited by K. Binder (Springer, New York, 1978).

[33]K. Binder, Phys. Rev. Lett. **47**, 693 (1981); Z. Phys. B **43**, 119 (1981).

[34]K. Binder, Z. Phys. B **45**, 61 (1981).

[35]M. E. Fisher, in *Proceedings of the International Summer School, Enrico Fermi, 1970, Course 51, Varenna, Italy,* edited by M. S. Green (Academic, New York, 1971).

[36]A. E. Ferdinand and M. E. Fisher, Phys. Rev. **185**, 832 (1969); D. P. Landau, Phys. Rev. B **13**, 2997 (1976); **14**, 255 (1976).

[37]M. E. Fisher and A. N. Berker, Phys. Rev. B **26**, 2507 (1982). See also V. Privman and M. E. Fisher, J. Stat. Phys. **33**, 385 (1983); K. Binder and D. P. Landau, Phys. Rev. B **30**, 1477 (1984), and references therein.

[38]J. Stephenson, Phys. Rev. B **1**, 4405 (1970).